Published in final edited form as:
Nat Struct Mol Biol. 2013 January ; 20(1): 29–35. doi:10.1038/nsmb.2446.

Structural plasticity of histones H3-H4 facilitates their allosteric exchange between RbAp48 and ASF1

Wei Zhang[#,1], **Marek Tyl**[#,1], **Richard Ward**[2], **Frank Sobott**[3], **Joseph Maman**[1], **Andal S. Murthy**[1], **Aleksandra A. Watson**[1], **Oleg Fedorov**[4], **Andrew Bowman**[5], **Tom Owen-Hughes**[5], **Hassane EL-Mkami**[6], **Natalia V. Murzina**[1], **David Norman**[2], and **Ernest D. Laue**[§,1]

[1]Department of Biochemistry, University of Cambridge, 80 Tennis Court Road, Cambridge, CB2 1GA, United Kingdom

[2]Nucleic Acids Research Group, School of Life Sciences, MSI/WTB Complex, Dow St., Dundee, DD1 5EH, United Kingdom

[3]Department of Chemistry, Centre for Proteomics, University of Antwerp, Groenenborgerlaan 171, 2020 Antwerp, Belgium

[4]The Structural Genomics Consortium, University of Oxford, Old Road Campus Research Building, Roosevelt Drive, Oxford, OX3 7DQ, United Kingdom

[5]Wellcome Trust Centre for Gene Regulation and Expression, College of Life Sciences, University of Dundee, Dundee, DD1 5EH, United Kingdom

[6]Millimetre wave and EPR Group, School of Physics and Astronomy , University of St Andrews, North Haugh, St Andrews, KY16 9SS, United Kingdom

Abstract

The mechanisms by which histones are disassembled and reassembled into nucleosomes and chromatin structure during DNA replication, repair and transcription are poorly understood. A better understanding of the processes involved is, however, crucial if we are to understand whether and how histone variants and post-translationally modified histones are inherited in an epigenetic manner. To this end we have studied the interaction of histones H3–H4 with the human retinoblastoma-associated protein RbAp48 and their exchange with a second histone chaperone, anti-silencing function protein 1 (ASF1). Exchange of histones H3–H4 between these two histone chaperones plays a central role in the assembly of new nucleosomes and we show here that the H3–H4 complex has a surprising structural plasticity, which is important for this exchange.

In all eukaryotes DNA is wrapped around an octamer of histone proteins to form nucleosomes, which fold to form higher order chromatin structures. The nucleosome comprises two copies of both histones H3 and H4, which form a heterotetramer and bind DNA in the first step of nucleosome assembly. This $(H3–H4)_2$ – DNA complex (the tetrasome) subsequently binds two histone H2A–H2B heterodimers to form the nucleosome core particle (refs. 1, 2). There are distinct variants of H2A, H2B, and H3, and all histones can also be post-translationally modified in multiple ways. The assembly of nucleosomes with variant and post-translationally modified histones at particular genomic locations is

[§]Corresponding author: e.d.laue@bioc.cam.ac.uk.
[#]These authors contributed equally to the work.

Author Contribution Section W.Z., M.T., R.W., F.S., J.M., A.A.W., and O.F. performed experiments. A.S.M. expressed recombinant RbAp48 protein. A.B, T.O.H, H.E.M., N.V.M., and D.N. provided technical and conceptual advice. E.D.L. supervised the work and prepared the manuscript, with assistance from the other authors.

Europe PMC Funders Author Manuscripts

thought to constitute a “histone code” that can be inherited in an epigenetic manner during DNA replication to establish and maintain transcriptional programs and cell identity (ref. 3).

When DNA is replicated, nucleosomes need to be disassembled in front of the replication fork and the histones must then be transferred to the newly duplicated strands for reassembly. Early biochemical studies showed that during DNA replication the ‘old’ parental nucleosomes segregate randomly onto the leading and lagging strands behind the replication fork, with the gaps being filled by the deposition of ‘new’ nucleosomes. Importantly, work from several groups using different approaches has shown that H3–H4 complexes involving the replication-dependent histone H3 variant (H3.1) are segregated as tetramers, i.e. a mixture of ‘old’ and ‘new’ histone H3–H4 dimers are not used to generate new nucleosomes during DNA replication (refs. 4, 5). This view has recently been reaffirmed by mass spectrometry studies that show that H3.1–H4 nucleosomes contain either ‘old’ or ‘new’ H3–H4 tetramers, but not a mixture (ref. 6). Surprisingly, however, studies of the *in-vivo* composition of histone H3 complexes (ref. 7), as well as structural studies of the ASF1–H3–H4 complex (refs. 8, 9), have shown that histone H3–H4 complexes are handled as dimers (for a review see ref. 10). To understand how histones H3–H4 are disassembled and reassembled we are studying their interactions with the retinoblastoma-associated proteins, RbAp46 and RbAp48, histone chaperones that are key players in the assembly of nucleosomes.

RbAp46 and RbAp48 are highly homologous (90 % identical) members of the WD40 repeat β-propeller structure proteins. RbAp46 is an essential subunit of the HAT1 histone-acetyltransferase complex, which acetylates newly synthesized histone H4 on lysines 5 and 12 prior to nucleosome assembly (refs. 11, 12). RbAp48 on the other hand is a subunit of the chromatin-assembly factor-1 (CAF-1) complex, which assembles histones H3 and H4 onto newly replicated DNA to initiate nucleosome assembly (refs. 13, 14). In addition to playing an essential role in replication-dependent nucleosome assembly, both RbAp46 and RbAp48 are also found in numerous other protein complexes involved in the regulation of chromatin structure. These include: the *Drosophila* nucleosome remodeling complex (NURF; refs. 15, 16); the nucleosome remodeling and deacetylase complex (NuRD; refs. 17, 18); and the polycomb repressive complex 2 (PRC2; ref. 19). Both NuRD and PRC2 play key roles in maintaining the silent state of master regulatory genes during embryonic development and stem cell renewal (refs. 20, 21), and studies of an *Arabidopsis* homologue, AtMSI1, suggest that RbAp48 also plays an important role in epigenetic inheritance during cell division (ref. 22).

In all of these different protein complexes RbAp46 and RbAp48 appear to act as chaperone proteins that bind to histone H3–H4 complexes, although we note that RbAp48 and p55 (the *Drosophila* homolog of RbAp46 or RbAp48) also bind to FOG-1 (Friend of GATA 1, ref. 23) and one of the subunits from the *Drosophila* PRC2 complex (Suz12, ref. 24), respectively. Previous studies have shown how RbAp46 and p55 interact with the N-terminal helix within the core histone-fold of H4 (refs. 25, 26). More recently p55 has also been shown to interact with the N-terminal tail of histone H3 (refs. 24, 27). However, despite their very central role, little is known about how RbAp46, RbAp48 or p55 function in chromatin-associated processes. It is not even clear whether they interact with the intact histone H3–H4 complex, or just with the isolated histone H3 or H4 proteins. Here we demonstrate that RbAp48 does indeed bind the histone H3–H4 complex. We also show that there are major structural rearrangements in the core fold of the histone H3–H4 complex when it binds RbAp48. Importantly, these results suggest that RbAp48 binding leads to conformational changes within the H3–H3 interface such that it only binds to H3–H4 dimers, rather than $(H3–H4)_2$ tetramers. Our studies suggest a surprising degree of structural plasticity in the core histone H3–H4 structure and we show that an allosteric mechanism

facilitates the exchange of H3–H4 between the RbAp48 and ASF1 histone chaperones. The finding that RbAp48 binds histone H3–H4 heterodimers, but *not* histone $(H3–H4)_2$ heterotetramers, has important implications for understanding the role(s) of these proteins and of histones H3–H4 in epigenetic inheritance.

Results

Stoichiometry of the RbAp48 interaction with H3–H4

Previously, we showed that both H3 and H4 interact with RbAp46 using gel filtration and cross-linking experiments (ref. 26). However, these experiments did not exclude the possibility that RbAp46 interacts with only one of these histones at a time.

To investigate this further, we performed gel filtration experiments using RbAp48 and globular forms of H3 (gH3) and H4 (gH4), which lack the parts of their flexible N-terminal tails (the first 26 and 19 residues of H3 and H4, respectively). [We studied the RbAp48–gH3–gH4 complex because it gave better resolved nano-electrospray ionization (ESI) mass spectra under non-dissociating conditions, and the N-terminal tails of H3 and H4 are not required for CAF-1-mediated nucleosome assembly (refs. 28, 29).] The N-terminus of unmodified H4 does not interact with RbAp46 or RbAp48 (refs. 12, 26, 27), but newly synthesized H4 is di-acetylated at Lys-5 and Lys-12 by RbAp46–HAT1 prior to binding ASF1. Therefore, we also confirmed that an N-terminal Lys5–Lys12 di-acetylated H4 peptide did not bind either RbAp48 or ASF1 (Supplementary Fig. 1). Size exclusion chromatography experiments showed that the RbAp48–gH3–gH4 complex migrates only marginally faster through a gel filtration column than does the tetrameric $(gH3–gH4)_2$ complex alone (Fig. 1a). This is consistent with disruption of the $(gH3–gH4)_2$ tetramer (44.3 kDa) upon binding RbAp48, giving a 1:1 (RbAp48 : gH3–gH4) complex (70 kDa), substantially smaller than that expected for RbAp48 binding a $(gH3–gH4)_2$ tetramer (92 kDa). A similar result is observed for ASF1, where the 1:1 human $ASF1^{1-159}$: gH3–gH4 complex (40 kDa) migrates through a gel filtration column more slowly than does the tetrameric $(gH3\text{-}gH4)_2$ complex alone (44.3 kDa, Supplementary Fig. 2). This suggested that, as with ASF1, RbAp48 might bind to gH3–gH4 heterodimers, as opposed to $(gH3–gH4)_2$ heterotetramers, forming a 1:1 RbAp48 : H3–H4 complex.

To verify whether RbAp48 binds H3–H4 heterodimers, we recorded nano-ESI mass spectra of the RbAp48–gH3–gH4 complex under non-dissociating conditions (Fig. 1b). Expansion of the m/z 3500 – 5500 region of the spectrum shows charge state series consistent with the masses of RbAp48–gH3–gH4, RbAp48–gH3 and RbAp48–gH4 (Fig. 1b). Importantly, no peaks consistent with the interaction of RbAp48 with a $(gH3–gH4)_2$ tetramer were observed – even when we tuned the mass spectrometer to favour the observation of larger complexes. This suggests that RbAp48 exists in a 1:1 complex with gH3–gH4, where both H3 and H4 can dissociate to yield either RbAp48–gH3 or RbAp48–gH4 sub-complexes (Fig. 1b). In an MS/MS experiment where a single charge state of the RbAp48–gH3–gH4 complex was fragmented by collision-induced dissociation with inert gas molecules, the gH4 protein dissociated from the complex more readily than gH3 (Fig. 1c). This either suggests that H3 associates more tightly with RbAp48, or that H4 is more exposed than H3 on the complex surface. Fragmentation of the RbAp48–gH3–gH4 complex always yielded some RbAp48–gH3 complex, demonstrating that the H3 globular domain interacts directly with RbAp48. This rules out the possibility that H3 interacts with RbAp48 solely through the H3 N-terminal tail (because this experiment was carried out with tailless gH3) or via interactions with H4. We also carried out similar experiments using intact H3 and H4 and, again, no evidence for an interaction of RbAp48 with a H3–H4 tetramer could be found (Supplementary Fig. 3). However, these studies did demonstrate that the intact H3–H4 complex interacts more stably with RbAp48 than the gH3–gH4 complex does, consistent

with reports that the H3 N-terminal tail binds the *Drosophila* RbAp48 homologue p55 (refs. 24, 27).

RbAp48 binds histone H3–H4 dimers

These above experiments suggested that RbAp48 interacts with H3–H4 dimers, but not $(H3–H4)_2$ tetramers. We next performed pulsed electron-electron double resonance (PELDOR) experiments to study the structure of H3–H4 when bound to RbAp48. PELDOR experiments allow the measurement of distances in the range of 20-80 Å or longer between two spin-labeled cysteine residues. These labels were incorporated into full-length unmodified H3–H4 via site-directed mutagenesis at positions where side chains are solvent-exposed and are not required for structural integrity (ref. 30).

First, an H3–H4 complex was studied wherein H3 had been labeled with an MTSL [(1-oxyl-2,2,5,5-tetramethylpyrroline-3-methyl)-methanethiosulfonate] spin-label at a cysteine introduced at Gln-125 (Fig. 2a). As shown previously, PELDOR experiments with the $(H3–H4)_2$ tetramer clearly show a peak at just less than 30 Å, consistent with the distance expected between the two H3 Gln-125 residues (ref. 31). When RbAp48 was added, however, very little interaction between the two spin-labels could be observed. Once again this suggests that RbAp48 disrupts $(H3–H4)_2$ heterotetramer formation when it binds H3–H4 heterodimers – when bound to RbAp48, the spin-labeled cysteines of each H3 molecule are no longer close enough in space to generate a PELDOR signal (Fig. 2a). Additionally, the normalized intensity (NI) of the data for the Gln-125 labeled H3–H4 tetramer (black trace in Fig. 2a) shows an oscillation depth of approximately 0.65, which suggests the interaction of two spins (ref. 32). By contrast, upon addition of RbAp48, the oscillation depth increases to ~0.85, indicating that there are very few interacting spin-labels (blue trace in Fig. 2a). Consequently, and consistent with the gel filtration and non-denaturing MS results, both the distance distributions and the oscillation depth of the PELDOR data suggest that RbAp48 binds H3–H4 dimers. These results were further supported by a second experiment investigating the interaction of RbAp48 with intact H3–H4 labeled at Gln-125 in H3 and Thr-71 in H4 (black trace in Fig. 2b). In the absence of RbAp48 the oscillation depth was 0.45 (consistent with more than two interacting spins) and we observed a broad multiple distance distribution as expected for the three spin-label distances in $(H3–H4)_2$ tetramers. When RbAp48 was added, the oscillation depth increased to 0.6, which is consistent with a decrease in the number of interacting spins (blue trace in Fig. 2b) and an RbAp48 interaction with H3–H4 dimers. This experiment further suggested that the structure of H3 at the H3–H3 dimerization interface (i.e. around Gln-125) is disrupted and becomes more dynamic when RbAp48 binds, because the transformed data suggest a number of different distances (Fig. 2b).

Taken together, these results all suggest that RbAp48 forms a 1:1 complex with H3–H4, i.e. that RbAp48 binds an H3-H4 heterodimer. The PELDOR data further suggest that RbAp48 binding destabilizes the structure of the H3-H3 interface in the (H3–H4)2 heterotetramer.

H3–H4 show large structural rearrangements on binding RbAp48

The non-denaturing MS analysis showed conclusively that RbAp48 can simultaneously interact with both H3 and H4 in the RbAp48–H3–H4 complex. We confirmed that RbAp48 binds H4 in a similar manner to RbAp46 and p55 (Supplementary Fig. 4) and next attempted to investigate the mode of interaction of the H3–H4 complex with RbAp48. Thus far it has not been possible to either crystallize the RbAp46 or RbAp48 complexes nor to obtain good quality NMR spectra, but the structures of RbAp46 and p55 in complex with an H4 peptide indicate that unfolding of helix-1 of the H4 core histone fold is necessary for interaction with RbAp46 or RbAp48 (refs. 25, 26). This suggests a model (Fig. 3a) where H3–H4 exists

in two different conformations: in one, H4 helix-1 is bound to the H3–H4 globular domains resulting in an H3–H4 conformation that cannot bind RbAp46 or RbAp48; in the other, H4 helix-1 is unfolded, permitting binding to RbAp46 and RbAp48.

We tested whether such a structural rearrangement can be observed during formation of the RbAp48–H3–H4 complex using PELDOR experiments. H4 was labeled at residue 25 and H3 was labeled at residue 65. We also used a C110E mutant of H3 to reduce any residual propensity for H3–H4 tetramerization (ref. 33). A rather broad distance distribution at ~29 Å (black trace) was observed for the doubly labeled H3–H4 heterodimer, which shifted to ~53 Å (blue trace) when H3–H4 was bound to RbAp48 (Fig. 3b). Confirmation of the previous result was obtained a similar result (where the peak shifts from ~23 Å to ~61 Å, Fig. 3c) when H3 was instead labeled at residue 90. These measured H3–H4 distances are consistent with a model (Fig. 3a), where H4 helix-1 is disengaged from the core histone fold in the RbAp48–H3–H4 complex. We see multiple peaks in the EPR data for both the H3–H4 and the RbAp48–H3–H4 complexes, suggesting that there is some conformational heterogeneity in both complexes, perhaps due to flexibility of the spin-label attached to residue 25 in H4 (which is unstructured in the RbAp46–H4 complex; refs. 25, 26).

RbAp48 and ASF1 can simultaneously interact with H3-H4

Previous structural studies have shown that ASF1 interacts with the C-terminal regions of H3 and H4 (refs. 8, 9) whereas RbAp46 and p55 interact with H4 helix-1 (refs. 25, 26). This suggests that RbAp46 or RbAp48 and ASF1 might be able to bind simultaneously to opposite sides of the H3–H4 dimer. To test this, we performed further gel filtration and non-denaturing ESI MS experiments. A refolded gH3–gH4 complex was mixed with RbAp48 in a 1:1 ratio together with an excess of $ASF1^{1\text{-}159}$ (18.1 kDa) and the complexes were analyzed by gel filtration. We found that a RbAp48–gH3–gH4–$ASF1^{1\text{-}159}$ quaternary complex can be formed (88 kDa), which elutes earlier from the column than either RbAp48–gH3–gH4 or $ASF1^{1\text{-}159}$–gH3–gH4 (retention volumes of 1.47 mL compared with 1.50 mL and 1.59 mL, respectively; compare Fig. 4a with Figs. 1a and Supplementary Fig. 2). The formation of this complex was further confirmed by gel filtration of intact H3–H4, mixed with $ASF1^{1\text{-}159}$ in a 1:1 molar ratio together with an excess of RbAp48 (Supplementary Fig. 5a). Under the same conditions, RbAp48 and ASF1 do not by themselves interact (Supplementary Fig. 5b), thus confirming that RbAp48–H3–H4–ASF1 complex formation is mediated by the histones (ref. 34).

RbAp48–H3–H4–ASF1 complex formation was further confirmed by non-denaturing ESI MS (Fig. 4b). Species were identified from RbAp48–H3–H4–ASF1, RbAp48 and ASF1, but not from RbAp48 or ASF1 with histones, suggesting that interactions of H3–H4 with both chaperones are destabilized in the presence of the other. (This may in turn lead to a loss of H3–H4 from solution under the lower salt conditions used for mass spectrometry.)

Allosteric model for exchange of H3–H4 between ASF1 and RbAp48

During nucleosome assembly ASF1 is thought to pass H3–H4 to RbAp48 (when part of CAF-1) for subsequent deposition on to DNA (reviewed in ref. 35). Our non-denaturing MS studies suggested that interactions of H3–H4 with both chaperones are destabilized in the presence of the other, and the EPR experiments further suggested that the H3–H3 dimerization interface – the region that binds ASF1 – is destabilized within RbAp48–H3–H4. This suggests that binding of RbAp48 to H3–H4 should destabilize the interaction with ASF1, thereby facilitating the exchange of H3–H4 between the two chaperones. To directly test this hypothesis we carried out fluorescence polarization (FP) experiments to compare the affinity of ASF1 for the H3–H4 and RbAp48–H3–H4 complexes.

First, the affinities of both ASF1 and RbAp48 for H3–H4 were measured, where H3 had either been labeled with the Cy3 fluorophore at Gln-125 (for measurement of the affinity of ASF1 binding) or at Leu-65 (for measurement of the affinity of RbAp48 binding). We labeled H3 at different positions in order to determine the affinities using fluorescence intensity experiments (data not shown). ASF1 and RbAp48 bound H3–H4 with very similar affinities – the apparent K_D values were 0.27 ± 0.11 nM and 0.61 ± 0.49 nM, respectively (Figs. 5a, b). At the concentrations of H3–H4 used in these experiments (20 nM for the ASF1 and 6 nM for the RbAp48 titrations, respectively), H3–H4 is present as a dimer (ref. 36), simplifying the analysis.

We then repeated the ASF1 experiment, this time after adding RbAp48 to Q125 Cy3-labelled H3–H4 at a concentration 10 fold higher than its K_D for binding to H3–H4. This showed that the affinity of ASF1 for the RbAp48–H3–H4 complex was substantially lower than that for H3–H4 alone – the apparent K_D was 7.1 ± 3.6 nM. To improve the statistics, we performed the fit using a Monte Carlo algorithm where we corrected for a slight drift. This gave a lower apparent K_D of 3.0 nM (error analysis was not possible using this approach), but both fitting procedures clearly indicate that the affinity of ASF1 for RbAp48–H3–H4 is an order of magnitude weaker than that for H3–H4 alone (Fig. 5c). The apparent K_D for binding of ASF1 to H3–H4 presented here (0.27 ± 0.11 nM) is lower than that of 2.5 nM for the binding of intact yeast Asf1 to H3–H4 determined by Donham et. al. (ref. 36). This discrepancy could reflect the species difference, or the different solution conditions or fluorescence method used. We repeated the whole experiment using separately purified proteins and measured apparent K_D values of 0.3 nM and 6.8 nM respectively for binding of ASF1 to H3–H4 and RbAp48–H3–H4, demonstrating the reproducibility of our apparent K_D values (data not shown). We also checked the apparent K_D for the binding of RbAp48 to H3–H4 using a different, FRET-based, approach and obtained a similar affinity (4.7 nM, data not shown). The fact that we can determine similar apparent K_D values using different fluorescence-based approaches gave us confidence in these findings.

Our results show that binding of RbAp48 to the histone H3–H4 complex destabilizes the interaction of ASF1 with H3–H4. This reduction in affinity of ASF1 for H3–H4, when complexed with RbAp48, suggests that RbAp48 modifies the H3–H4 structure, reducing its affinity for ASF1 by an allosteric mechanism. This would facilitate transfer of H3–H4 from ASF1 to RbAp48 in CAF-1-mediated nucleosome assembly. In other words, when ASF1–H3–H4 binds to RbAp48, this weakens the interaction of H3–H4 with ASF1, allowing the latter's release.

Discussion

Recent purification of histone H3 complexes formed during the assembly and processing of histone H3–H4 has identified a number of distinct complexes on which H3–H4 are assembled. During the course of assembly, 'new' H4 is acetylated on Lys-5 and Lys-12 through interactions with RbAp46-HAT1 before being transferred to ASF1 (refs. 35, 37). Following nuclear import, the replication dependent H3–H4 complex (H3.1-H4) is transferred from ASF1 to CAF-1 (ref. 7), which consists of RbAp48 in a complex with p60 and p150 (refs. 13, 14), for subsequent deposition onto DNA (reviewed in ref. 35). Previous studies have shown that ASF1 interacts directly with the p60 subunit of CAF-1 (ref. 38) to deliver the H3–H4 complex to RbAp48 in CAF-1. Thus RbAp46 and RbAp48 interact with the H3–H4 complex and ASF1 at two key stages of the pathway for deposition of newly synthesized H3–H4 during replication-dependent nucleosome assembly. (We note that these complexes also involve other chaperones, which for simplicity are not discussed here – see ref. 37.)

Using gel filtration and non-denaturing mass spectrometry we have shown that RbAp48 makes direct contacts with both histones H3 and H4 in the H3–H4 complex. Our EPR experiments suggest a surprising plasticity in the H3–H4 complex, with a structural rearrangement consistent with helix-1 in H4 becoming disengaged from the core H3–H4 fold in order to bind to RbAp48. Moreover, gel filtration, non-denaturing MS and EPR experiments all show that RbAp48 interacts with H3–H4 dimers, but not with histone $(H3–H4)_2$ tetramers, and the EPR data suggest that this is because the H3–H3 interface is destabilized. These results suggest an allosteric model for the exchange of histones H3–H4 between the two chaperone proteins, whereby RbAp48 binding to H3–H4 weakens its interactions with ASF1. We obtained direct evidence for this model by comparing the binding affinities of ASF1 to either the H3–H4 or RbAp48–H3–H4 complexes using fluorescence polarization experiments. Because histones bind so tightly to these chaperones it seems likely that the structural plasticity of H3–H4, and the allosteric mechanism that releases ASF1 when ASF1–H3–H4 binds to RbAp48, is functionally important for the transfer of these histones between the different complexes involved in chromatin assembly. In the future it will also be interesting to carry out similar experiments with RbAp46, which instead transfers H3–H4 *to* ASF1.

A picture is thus emerging of dimeric histone H3–H4 complexes being exchanged between a series of chaperone complexes prior to their deposition onto nascent DNA. However, H3–H4 tetramers need to be formed at some point. Our results suggest that newly synthesized H3–H4 complexes are handled as dimers at all points up until tetramer assembly on CAF-1. Alternatively, assembly of new nucleosomes during DNA replication might occur via sequential CAF-1 mediated deposition of two H3–H4 dimers onto DNA, a possibility that needs to be tested in future experiments. The finding that RbAp46 and RbAp48 bind to histone H3–H4 dimers, but not to histone H3–H4 tetramers, may have wider implications because RbAp46, RbAp48 and their homologues function in a very large number of complexes involved in chromatin assembly, remodeling and modification, and it suggests that in many other chromatin related processes histones H3–H4 might be handled as dimers. More generally, it seems plausible that the presence of RbAp46 or RbAp48 in a diverse range of chromatin related complexes may reflect a requirement for reconfiguring the H3–H4 fold in processes that include the post-translational modification of histones and the repositioning of nucleosomes.

Our findings also have a number of potentially important implications for the epigenetic inheritance of post-translationally modified versions of H3–H4. It is thought that during DNA replication nucleosomes are completely disassembled at the replication fork and that ASF1, which can only bind to a dimer of H3–H4, is involved in the disassembly process through its association with the MCM2-7 helicase (ref. 39). However, as discussed above all the evidence suggests that parental $(H3–H4)_2$ is segregated as a tetramer during DNA replication (reviewed in ref. 10). For H3–H4 to segregate to the leading and lagging DNA strands as tetramers, parental histones need to be transferred from in front of the replication fork and re-deposited in a process that excludes the incorporation of newly synthesized H3–H4 dimers. This could perhaps be facilitated by the localization of both ASF1 and CAF-1 to the replication fork, through their interactions with the MCM2-7 helicase (ref. 39) and PCNA (ref. 40), respectively, such that when ASF1–H3–H4 dissociates the histones have a greater tendency to bind to a CAF-1 complex that is in close spatial proximity. However, the assembly of “new” nucleosomes might be somehow separated from the segregation of “old” nucleosomes from in front to behind the replication fork. For example, the latter process could involve histone chaperones that are known to bind H3–H4 as tetramers (see e.g. ref. 41), or it might involve some form of temporal separation.

Online Methods

Protein expression and purification

Recombinant RbAp48 and ASF1$^{1-159}$ proteins were expressed and purified as described (refs. 23 and 37, respectively). Histones H3 and H4 (*Xenopus leavis*), both full-length and globular domain (gH3, residues 27-135; gH4, residues 20 –102) were expressed, purified and refolded as described in ref. 2.

Protein complex formation and size-exclusion chromatography

RbAp48, ASF1$^{1-159}$ and refolded histone $(H3–H4)_2$ tetramers (either by themselves or as complexes prepared by mixing the appropriate components in 0.5 M NaCl), were run in 20 mM HEPES pH 7.5, 0.7 M NaCl, and 1 mM EDTA at 4 °C on a Superdex 200 PC 3.2 /30 analytical size-exclusion column connected to an Ettan LC system (GE healthcare). Fractions (80 μL) were collected and the resulting proteins were analyzed on 4-12 % NuPAGE gels (Invitrogen). The apparent molecular masses of the complexes were estimated by interpolation from a standard linear regression curve.

BioLayer Interferometry

BioLayer Interferometry (BLI) experiments were performed on a 16 channel ForteBio Octet RED 384 plate analysis instrument at 20 °C in 25 mM HEPES pH 7.5 and 100 mM NaCl, using either 20 μM RbAp48 or ASF1. The data were processed with the Overlord3 laboratory automation control software.

Non-denaturing mass spectrometry analysis

Samples were buffer-exchanged into 200 mM ammonium acetate pH 7.0 prior to mass spectrometry analysis and were typically measured at concentrations of 5-20 μM. Nano-electrospray ionization (nano-ESI) was performed using a chip-based infusion device (Advion Nanomate Triversa) with a spray voltage of 1.7-1.8 kV coupled to a Q-TOF mass spectrometer (Waters Synapt G1 T-wave IMS-MS/MS). Interface conditions on the mass spectrometer were chosen to effect gentle desolvation of native structures while maintaining non-covalent interactions in the complexes (ref. 43). Key experimental parameters were (mobility mode): sample and extractor cone voltages of 60-120 V and 0-1 V, respectively; trap and transfer collision energies of 6-25 V and 4-15 V, respectively; bias 15-30 V; and backing, source, trap and IMS pressures of 5e0, 5e-3, 3e-2, 5e-1 mbar, respectively. Peak assignment was performed using the Masslynx 4.0 software and by manual fitting to calculated charge states.

Preparation of spin-labeled histone chaperone complexes

Spin-labeled H3-H4 complexes were prepared as described (refs. 44, 29) and mixed with concentrated RbAp48 to give 300 - 400 μM samples). These were exchanged into a buffer with 0.8 M sodium chloride made up in deuterium oxide, using multiple rounds of concentration and dilution in Amicon ultra centrifugal concentrators (Millipore). 50 μL of 97 % $^{2}H_8$-glycerol was added (Cambridge Isotope Laboratories) to give a final sodium chloride concentration of 0.4 M, prior to mixing and storage at -80 °C until measurement by EPR. Complexes containing ASF1 were prepared in the same way except that the buffer exchange was carried out in 1 M sodium chloride resulting in a final concentration of 0.5 M after addition of 50 % D_8-glycerol.

PELDOR experiments

PELDOR experiments were carried out using a Bruker ELEXSYS E580 spectrometer operating at the X-band with a dielectric ring resonator and a second 400 U Bruker

microwave source. All measurements were made at 50 K with an over coupled resonator giving a Q factor of approximately 100. The video bandwidth was set to 20 MHz. A four-pulse, dead-time free, PELDOR sequence was used with the pump pulse frequency positioned at the center of the nitroxide spectrum. The frequency of the observer pulses was increased by 80 MHz. The observer sequence used a 32 ns π-pulse and the pump π-pulse was typically 16 ns. The experiment repetition time was 4.08 ms, and the number of scans used was sufficient to obtain a suitable quality signal (typically >400 scans) with 50 shots at each time point.

PELDOR data analysis

In brief, the experimentally obtained time domain trace was processed so as to remove any unwanted intermolecular couplings arising from background decay. Tikhonov regularization was then used to simulate time trace data that gives rise to distance distributions, P(r), of different peak width depending on the regularization factor, alpha. The alpha term used was judged by reference to a calculated L curve. The L curve is a parametric plot that compares smoothness of the distance distribution to the mean square deviation. The most appropriate alpha term to be used is at the inflection of the L curve, as this provides the best compromise between smoothness (artifact suppression) and fit to the experimental data. PELDOR data were analyzed using the DeerAnalysis2006 software package (ref. 45). The dipolar coupling evolution data was corrected for background echo decay using a homogeneous three-dimensional spin distribution. The starting time for the background fit was optimized to give the best fit to the Pake pattern in the Fourier transformed data and the lowest root mean square deviation background fit.

Fluorescence polarization (FP) experiments

H3 was labeled with the Cy3 fluorescent dye (GE Healthcare) as described previously (ref. 46). H3 and H4 were then refolded into 10 mM Tris-HCl pH 7.5 and 2 M KCl. ASF1 was mixed with the H3–H4 complex to give maximum concentrations of the histone chaperone and Cy3-labeled H3–H4 of 200 nM and 20 nM, respectively, in 10 mM Tris-HCl pH 7.5, 150 mM KCl, 5 % glycerol, 0.01 % NP40 and 0.01 % CHAPS, prior to a serial dilution against the same buffer containing 20 nM Cy3-labeled H3–H4. (For the RbAp48 titration the H3–H4 concentration was 6 nM.) Fluorescence polarization measurements were recorded using a PHERAstar FS plate reader (BMG Labtech; Germany) equipped with a fluorescence polarization optical module (excitation = 540 nm; emission = 590 nm). The anisotropy was measured at 20°C in black 96-well half area, flat bottom, NBS plates (Corning; USA). The instrument was set in a top optical measurement mode, with 200 flashes per well. The gain and focal height were set using free fluorescein (Fluorescein Sodium; Fluka) in 50 mM Tris-HCl pH 8.0 (mP = 35). Samples were incubated at 20 °C for at least 5 minutes prior to measurement to allow the binding to reach equilibrium, and at least three independent experiments were performed for each sample.

FP experimental data analysis

The fluorescence anisotropy data were analyzed using a simple 1 to 1 binding model [RbAp48 does not interact directly with ASF1 (see Supplementary Fig. 4), and the H3–H4 complex exists as a dimer at the concentrations used (ref. 36)]. Because the Cy3-labeled H3–H4 concentrations used in our experiments (in order to ensure an acceptable signal to noise ratio) are substantially larger than the measured K_D values, we performed non-linear fits to the raw data of ligand depletion binding isotherms adapted for fluorescence anisotropy measurements (ref. 47, 48) using the pro*fit* package (Quantum Soft, Switzerland):

$$r_{obs}=r_0+\Delta r\frac{([D]_0+K_D+[P]_0)-\sqrt{([D]_0+K_D+[P]_0)^2-4[D]_0[P]_0}}{2[D]_0}$$

where: r_{obs} is the measured anisotropy, r_0 is the anisotropy of the Cy3-bound histone H3–H4 complex in the absence of ligand, Δr is the anisotropy amplitude of the ligand-saturated histone H3–H4 complex, $[D]_0$ is the total concentration of the ligand, $[P]_0$ is the total concentration of the Cy3-bound histone H3–H4 complex, and K_D is the dissociation equilibrium constant. For the titration of ASF1 with the RbAp48–H3–H4 complex a linear drift term was added to the equation above. The non-linear fits were initially performed using a Monte Carlo algorithm without error analysis and the fitted parameters were used for fitting with a Levenberg-Marquardt algorithm with error analysis. The resulting errors (1 standard deviation) are large because of the poor signal to noise. The quality of the fits were assessed by translating the Chi squared values into probabilities (P). Because the P value for the titration of ASF1 with the RbAp48–H3–H4 complex was low we repeated the fit using a Monte Carlo algorithm with a Lorentzian distribution of the errors to account for their non-Gaussian distribution (see Fig. 5c). The K_D values are reported as apparent K_D because the initial extent of ligand depletion exceeds 50 % of the K_D value (ref. 49). We estimate that the true K_D values are lower (*i.e.* the affinity is higher).

Supplementary Material

Refer to Web version on PubMed Central for supplementary material.

Acknowledgments

We thank I. Berger (European Molecular Biology Laboratory, Grenoble, France) for insect cell expression vectors, R. Marmostein (Wistar Institute, Philadelphia, P.A., U.S.A.) for the plasmid expressing human ASF1$^{1\text{-}159}$, K. Luger (Colorado State University, Colorado, C.O., U.S.A.) for advice on suitable buffers for fluorescence experiments, S. McLaughlin and N. Royle for purification of preliminary samples of histones H3-H4 and ASF1, A. Murzin for helpful discussions and comments on the manuscript, the PNAC facility for mass spectrometry and amino acid analysis, and J. McCullagh and C. Schofield (Chemistry Department, University of Oxford, U.K.) for access to the Synapt instrument for non-denaturing MS experiments. We thank the Wellcome Trust, the EPSRC and the BBSRC for their support of this research: 082010/Z/07/Z (EDL, NM) 092441/Z/10/Z (AAW), BB/D526088/1 (MT), EC FP7 277899 (EDL, FS), BB/E022286/1 (DGN, RW).

References

1. Gruss C, Wu J, Koller T, Sogo JM. Disruption of the nucleosomes at the replication fork. EMBO J. 1993; 12:4533–45. [PubMed: 8223463]
2. Luger K, Rechsteiner TJ, Flaus AJ, Waye MM, Richmond TJ. Characterization of nucleosome core particles containing histone proteins made in bacteria. J Mol Biol. 1997; 272:301–11. [PubMed: 9325091]
3. Strahl BD, Allis CD. The language of covalent histone modifications. Nature. 2000; 403:41–5. [PubMed: 10638745]
4. Prior CP, Cantor CR, Johnson EM, Allfrey VG. Incorporation of exogenous pyrenelabeled histone into Physarum chromatin: a system for studying changes in nucleosomes assembled in vivo. Cell. 1980; 20:597–608. [PubMed: 7417999]
5. Jackson V. Deposition of newly synthesized histones: hybrid nucleosomes are not tandemly arranged on daughter DNA strands. Biochemistry. 1988; 27:2109–20. [PubMed: 3378048]
6. Xu M, et al. Partitioning of histone H3-H4 tetramers during DNA replication-dependent chromatin assembly. Science. 2010; 328:94–8. [PubMed: 20360108]

7. Tagami H, Ray-Gallet D, Almouzni G, Nakatani Y. Histone H3.1 and H3.3 complexes mediate nucleosome assembly pathways dependent or independent of DNA synthesis. Cell. 2004; 116:51–61. [PubMed: 14718166]
8. English CM, Adkins MW, Carson JJ, Churchill ME, Tyler JK. Structural basis for the histone chaperone activity of Asf1. Cell. 2006; 127:495–508. [PubMed: 17081973]
9. Natsume R, et al. Structure and function of the histone chaperone CIA/ASF1 complexed with histones H3 and H4. Nature. 2007; 446:338–41. [PubMed: 17293877]
10. Annunziato AT. Split decision: what happens to nucleosomes during DNA replication? J Biol Chem. 2005; 280:12065–8. [PubMed: 15664979]
11. Parthun MR, Widom J, Gottschling DE. The major cytoplasmic histone acetyltransferase in yeast: links to chromatin replication and histone metabolism. Cell. 1996; 87:85–94. [PubMed: 8858151]
12. Verreault A, Kaufman PD, Kobayashi R, Stillman B. Nucleosomal DNA regulates the core-histone-binding subunit of the human Hat1 acetyltransferase. Curr Biol. 1998; 8:96–108. [PubMed: 9427644]
13. Smith S, Stillman B. Purification and characterization of CAF-I, a human cell factor required for chromatin assembly during DNA replication in vitro. Cell. 1989; 58:15–25. [PubMed: 2546672]
14. Verreault A, Kaufman PD, Kobayashi R, Stillman B. Nucleosome assembly by a complex of CAF-1 and acetylated histones H3/H4. Cell. 1996; 87:95–104. [PubMed: 8858152]
15. Martinez-Balbas MA, Tsukiyama T, Gdula D, Wu C. Drosophila NURF-55, a WD repeat protein involved in histone metabolism. Proc Natl Acad Sci U S A. 1998; 95:132–7. [PubMed: 9419341]
16. Barak O, et al. Isolation of human NURF: a regulator of Engrailed gene expression. EMBO J. 2003; 22:6089–100. [PubMed: 14609955]
17. Wade PA, Jones PL, Vermaak D, Wolffe AP. A multiple subunit Mi-2 histone deacetylase from Xenopus laevis cofractionates with an associated Snf2 superfamily ATPase. Curr Biol. 1998; 8:843–6. [PubMed: 9663395]
18. Zhang Y, et al. Analysis of the NuRD subunits reveals a histone deacetylase core complex and a connection with DNA methylation. Genes Dev. 1999; 13:1924–35. [PubMed: 10444591]
19. Kuzmichev A, Jenuwein T, Tempst P, Reinberg D. Different EZH2-containing complexes target methylation of histone H1 or nucleosomal histone H3. Mol Cell. 2004; 14:183–93. [PubMed: 15099518]
20. Kaji K, Nichols J, Hendrich B. Mbd3, a component of the NuRD co-repressor complex, is required for development of pluripotent cells. Development. 2007; 134:1123–32. [PubMed: 17287250]
21. Shen X, et al. Jumonji modulates polycomb activity and self-renewal versus differentiation of stem cells. Cell. 2009; 139:1303–14. [PubMed: 20064376]
22. Hennig L, Taranto P, Walser M, Schonrock N, Gruissem W. Arabidopsis MSI1 is required for epigenetic maintenance of reproductive development. Development. 2003; 130:2555–65. [PubMed: 12736201]
23. Lejon S, et al. Insights into association of the NuRD complex with FOG-1 from the crystal structure of an RbAp48.FOG-1 complex. J Biol Chem. 2011; 286:1196–203. [PubMed: 21047798]
24. Schmitges, Frank W., et al. Histone Methylation by PRC2 Is Inhibited by Active Chromatin Marks. Molecular cell. 2011; 42:330–341. [PubMed: 21549310]
25. Song JJ, Garlick JD, Kingston RE. Structural basis of histone H4 recognition by p55. Genes Dev. 2008; 22:1313–8. [PubMed: 18443147]
26. Murzina NV, et al. Structural basis for the recognition of histone H4 by the histone-chaperone RbAp46. Structure. 2008; 16:1077–85. [PubMed: 18571423]
27. Nowak AJ, et al. Chromatin-modifying complex component Nurf55/p55 associates with histones H3, H4 and Polycomb Repressive Complex 2 subunit Su(z)12 through partially overlapping binding sites J. Biol. Chem. 2011; 286:23388–96.
28. Ma XJ, Wu J, Altheim BA, Schultz MC, Grunstein M. Deposition-related sites K5/K12 in histone H4 are not required for nucleosome deposition in yeast. Proc Natl Acad Sci U S A. 1998; 95:6693–8. [PubMed: 9618474]

29. Shibahara K, Verreault A, Stillman B. The N-terminal domains of histones H3 and H4 are not necessary for chromatin assembly factor-1-mediated nucleosome assembly onto replicated DNA in vitro. Proc Natl Acad Sci U S A. 2000; 97:7766–71. [PubMed: 10884407]
30. Ward R, Bowman A, El-Mkami H, Owen-Hughes T, Norman DG. Long distance PELDOR measurements on the histone core particle. J Am Chem Soc. 2009; 131:1348–9. [PubMed: 19138067]
31. Bowman A, Ward R, El-Mkami H, Owen-Hughes T, Norman DG. Probing the (H3-H4)2 histone tetramer structure using pulsed EPR spectroscopy combined with site-directed spin labelling. Nucleic Acids Res. 2010; 38:695–707. [PubMed: 19914933]
32. Bode BE, et al. Counting the monomers in nanometer-sized oligomers by pulsed electron-electron double resonance. J Am Chem Soc. 2007; 129:6736–45. [PubMed: 17487970]
33. Banks DD, Gloss LM. Folding mechanism of the (H3-H4)2 histone tetramer of the core nucleosome. Protein Sci. 2004; 13:1304–16. [PubMed: 15096635]
34. Jasencakova Z, Groth A. Restoring chromatin after replication: how new and old histone marks come together. Semin Cell Dev Biol. 2010; 21:231–7. [PubMed: 19815085]
35. Ransom M, Dennehey BK, Tyler JK. Chaperoning histones during DNA replication and repair. Cell. 2010; 140:183–95. [PubMed: 20141833]
36. Donham DC 2nd, Scorgie JK, Churchill ME. The activity of the histone chaperone yeast Asf1 in the assembly and disassembly of histone H3/H4-DNA complexes. Nucleic Acids Res. 2011; 39:5449–58. [PubMed: 21447559]
37. Campos EI, et al. The program for processing newly synthesized histones H3.1 and H4. Nature Structural & Molecular Biology. 2010; 17:1343–51.
38. Tang Y, et al. Structure of a human ASF1a-HIRA complex and insights into specificity of histone chaperone complex assembly. Nature Structural & Molecular Biology. 2006; 13:921–9.
39. Groth A, et al. Regulation of replication fork progression through histone supply and demand. Science. 2007; 318:1928–31. [PubMed: 18096807]
40. Shibahara K, Stillman B. Replication-dependent marking of DNA by PCNA facilitates CAF-1-coupled inheritance of chromatin. Cell. 1999; 96:575–85. [PubMed: 10052459]
41. Bowman A, et al. The histone chaperones Nap1 and Vps75 bind histones H3 and H4 in a tetrameric conformation. Mol Cell. 2011; 41:398–408. [PubMed: 21329878]
42. DeLano, W. The PyMOL molecular graphics system. DeLano Scientific; Palo Alto, CA, USA: 2002.
43. Sobott F, McCammon MG, Hernandez H, Robinson CV. The flight of macromolecular complexes in a mass spectrometer. Philos Transact A Math Phys Eng Sci. 2005; 363:379–89. discussion 389-91. [PubMed: 15664889]
44. Ward R, Keeble DJ, El-Mkami H, Norman DG. Distance determination in heterogeneous DNA model systems by pulsed EPR. Chembiochem. 2007; 8:1957–64. [PubMed: 17886320]
45. Jeschke G, et al. DeerAnalysis2006—a comprehensive software package for analyzing pulsed ELDOR data. Applied Magnetic Resonance. 2006; 30:473–498.
46. Park YJ, Dyer PN, Tremethick DJ, Luger K. A new fluorescence resonance energy transfer approach demonstrates that the histone variant H2AZ stabilizes the histone octamer within the nucleosome. J Biol Chem. 2004; 279:24274–82. [PubMed: 15020582]
47. Kenakin, TP. Pharmacological analysis of drug receptor interaction. Raven Press; New York: 1987. p. 205-244.
48. Swillens S. Interpretation of Binding Curves Obtained with High Receptor Concentrations - Practical Aid for Computer-Analysis. Molecular Pharmacology. 1995; 47:1197–1203. [PubMed: 7603460]
49. Hulme EC, Trevethick MA. Ligand binding assays at equilibrium: validation and interpretation. British Journal of Pharmacology. 2010; 161:1219–1237. [PubMed: 20132208]

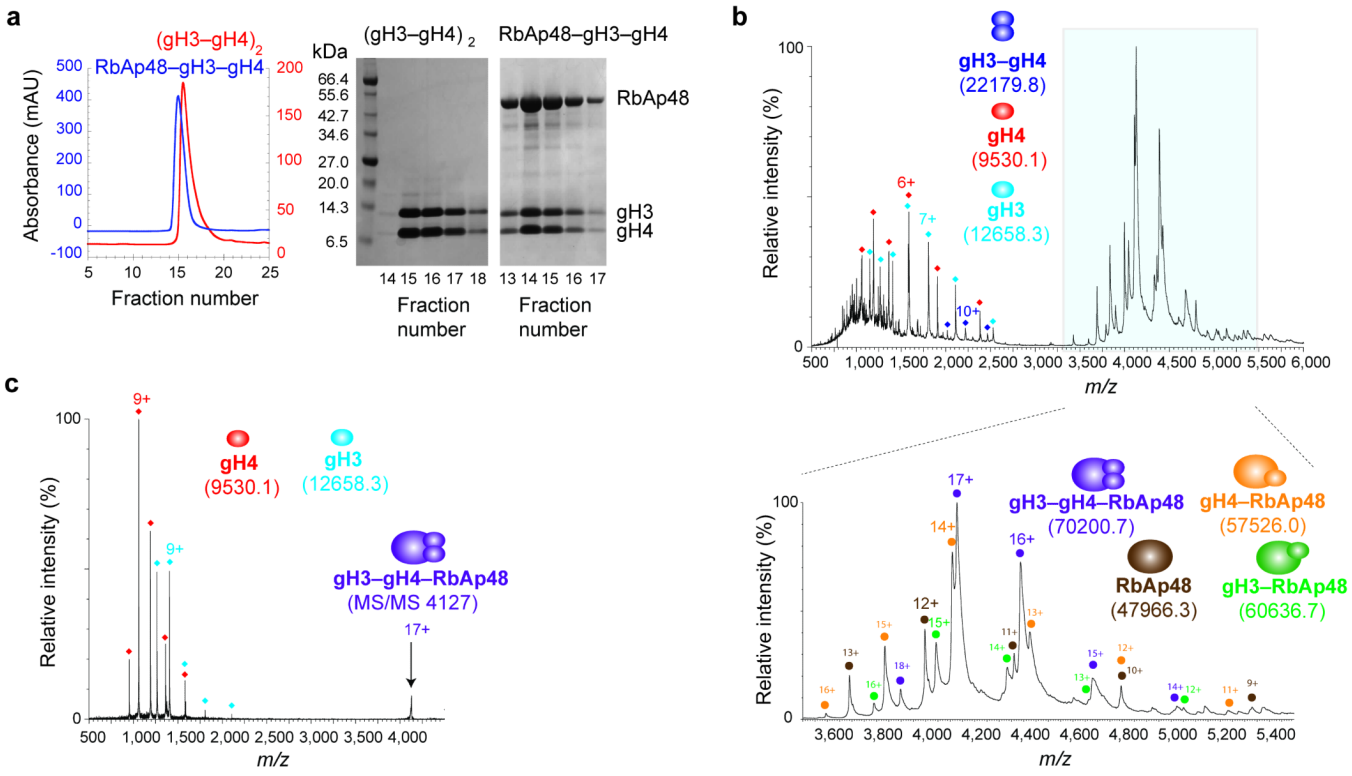

Figure 1.

Stoichiometry of the RbAp48 interaction with the histone H3–H4 complex. **a**, Refolded recombinant histones gH3 and gH4 were analyzed on a Superdex 200 size exclusion column, either alone (red trace), or in the presence of RbAp48 in a 1:1 ratio (blue trace). Eluted complexes were analyzed using SDS-PAGE gels (right). **b**, Non-denaturing nano-ESI mass spectrum of the RbAp48–gH3–gH4 complex. The m/z region 3500 to 5500 is expanded (below) to show the ion series for RbAp48–gH3–gH4 (~50 % of total intensity), RbAp48–gH3 (~20 %) and RbAp48–gH4 (~30 %), represented by purple, green and orange dots, respectively. **c**, The RbAp48–gH3–gH4 species was selected for collision-induced dissociation leading to release of either gH3 (~40 %) or gH4 (~60 %). (The remaining RbAp48–gH4 and RbAp48–gH3 complexes are above m/z 4500, and are not shown.) A comparison of the experimental vs theoretical m/z values is provided in the Supplementary Table.

Europe PMC Funders Author Manuscripts

Europe PMC Funders Author Manuscripts

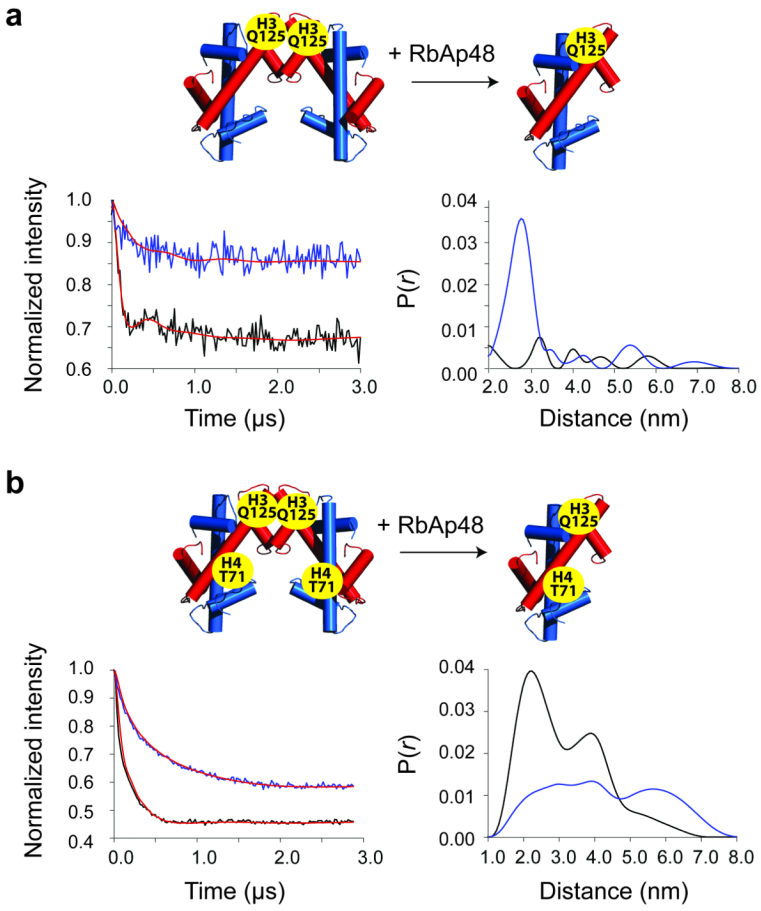

Figure 2.

RbAp48 binds to histone H3–H4 dimers. **a**, Background corrected PELDOR data for the H3Q125C spin-labeled $(H3–H4)_2$ complex alone (black), and following the addition of two equivalents of RbAp48 (blue) (left panel). Tikhonov derived distance distributions show a clear peak at ~30 Å for the H3Q125-labelled H3–H4 tetramer, but none for the RbAp48–H3–H4 complex (right panel). **b**, Background corrected PELDOR data for the H3–H4 complex, where both H3Q125C and H4T71C were spin-labeled, before (black) and after (blue) the addition of two equivalents of RbAp48 (left panel). Tikhonov derived distance distributions show peaks at ~20, 37 and 56 Å for the H3–H4 tetramer and several overlapping peaks for the RbAp48 complex (right panel). In both **a** and **b**, the most appropriate time trace simulation (obtained using Tikhonov regularization) is shown in red. A C110A mutation in H3 was used such that only the unique cysteine at Gln-125 was labeled with MTSL.

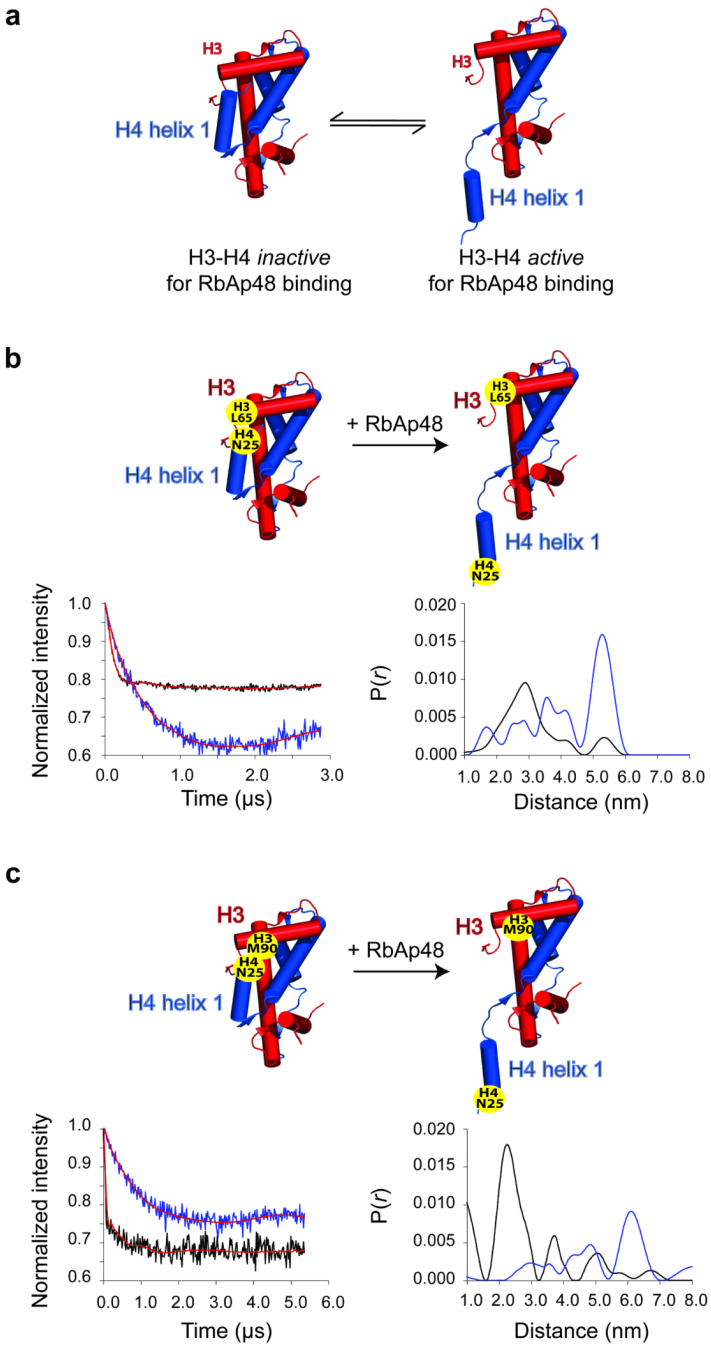

Figure 3.

The H3–H4 complex undergoes substantial structural rearrangement upon binding of RbAp48. **a**, Model of two possible conformations for H3–H4 in solution. The model was generated using PyMol (ref. 42). Helix-1 from H4 may unfold to interact with the RbAp46 and RbAp48 binding pocket as observed in the RbAp46–H4 crystal structure. **b**, Background corrected PELDOR data for an H3–H4 complex, where H3L65C and H4N25C were spin-labeled, before and after the addition of an equimolar amount of RbAp48 are shown in black and blue, respectively (left panel). Distance distribution peaks are observed for the H3–H4 dimer (~30 Å), and for the RbAp48 complex (~55 Å) (right panel). **c**,

Background corrected PELDOR data for an H3–H4 complex, where H3M90C and H4N25C were spin-labeled, before and after the addition of an equimolar amount of RbAp48 (black and blue, respectively, see left panel). The distance distribution shows a predominant peak for the H3–H4 dimer (~23 Å) and a major peak (~61 Å) for the RbAp48 complex (see right panel). In **b** and **c**, the most appropriate time trace simulation (obtained using Tikhonov regularization) is shown in red. A C110E mutation in H3 was used to reduce H3–H4 tetramerization and create an obligate H3-H4 dimer (ref. 33).

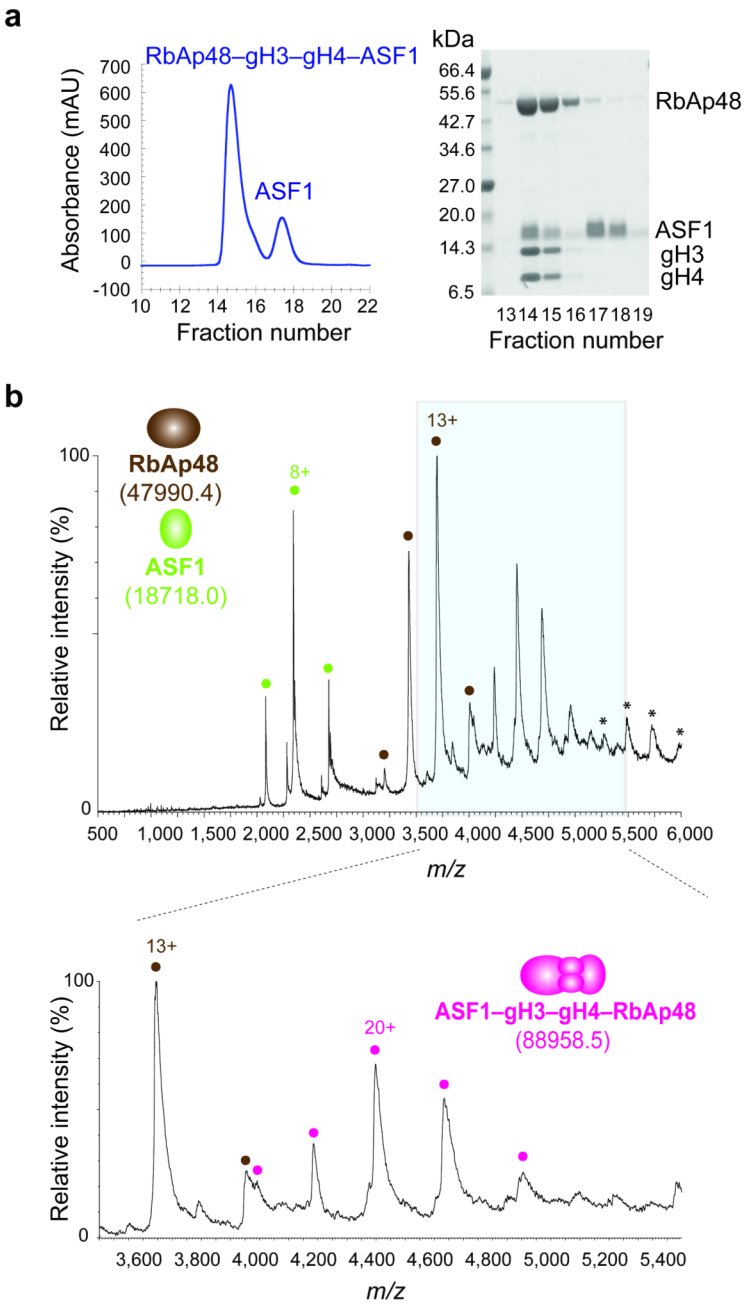

Figure 4.

Both RbAp48 and ASF1 can simultaneously bind the histone H3–H4 complex. **a**, gH3 and gH4 were refolded and mixed with RbAp48 in a 1:1 molar ratio together with excess ASF1$^{1\text{-}159}$ prior to analysis on a Superdex 200 size exclusion column. The eluted proteins were analyzed by SDS-PAGE (right panel). **b**, Non-denaturing nano-ESI mass spectrum of the RbAp48–gH3–gH4–ASF1$^{1\text{-}159}$ complex. The ion series from the RbAp48–gH3–gH4–ASF1$^{1\text{-}159}$, RbAp48, and ASF1$^{1\text{-}159}$ species are shown by magenta, brown, and light green diamonds, respectively. A comparison of the experimental vs theoretical m/z values is provided in the Supplementary Table. (The peak series marked with asterisks corresponds to a 1:2:2:2 RbAp48–H3–H4–ASF1$^{1\text{-}159}$ complex, which perhaps forms due to oxidation and dimerization of ASF1$^{1\text{-}159}$ in the sample.)

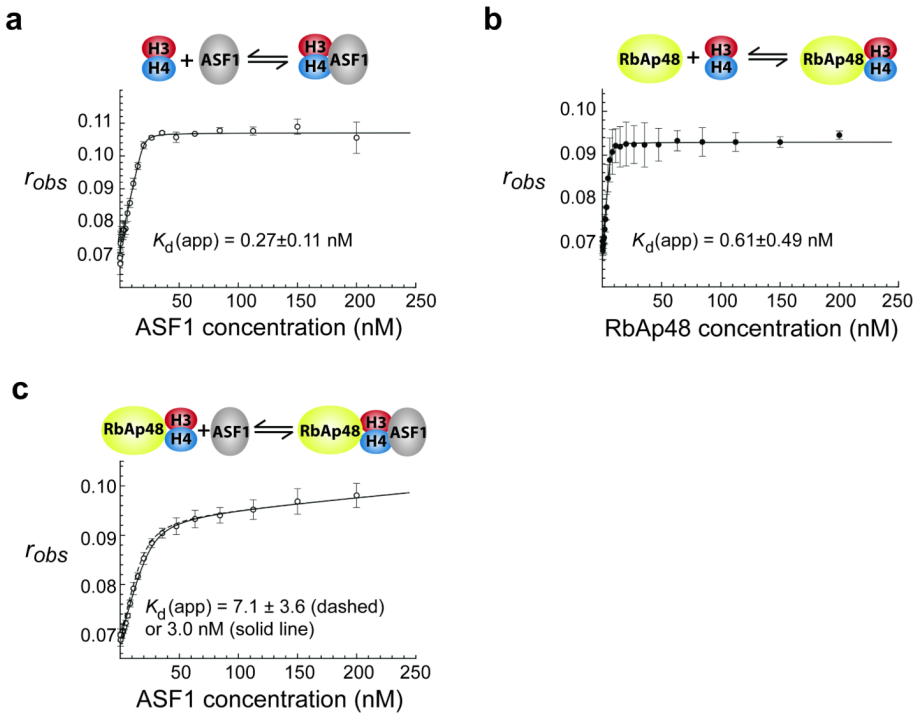

Figure 5.

Comparison of the affinities of ASF1 for the histone H3–H4 and RbAp48–H3–H4 complexes. **a,** and **b**, r_{obs}, the measured fluorescence anisotropy, is plotted against increasing concentrations of either ASF1$^{1\text{-}159}$ or RbAp48 to demonstrate binding to H3-H4. H3 was labeled with the Cy3 fluorophore at either Gln-125 or Leu-65. **c**, Plot of r_{obs} against increasing concentrations of ASF1$^{1\text{-}159}$ for binding to the RbAp48–H3–H4 complex, labeled with Cy3 at Gln-125 on H3. In **a**, and **b**, a ligand-depletion binding isotherm was fitted to the data using the Levenberg-Marquardt algorithm. In **c**, the data were fitted with either a ligand-depletion binding isotherm using the Levenberg-Marquardt algorithm (dashed line), or with an anisotropy ligand-depletion binding isotherm (with drift) using a Monte Carlo algorithm (solid line). (Note that in **b**, the concentration of Cy3-labeled H3–H4 was lower than that in **a** and **c**, giving the curves a different appearance) All experiments were carried out in triplicate – data points are the mean of three independent experiments and the error bars represent ± 1 standard deviation. A C110A mutation in H3 was used such that only the unique cysteine was labeled with the fluorophore.